



Structural, dielectric, linear and nonlinear optical parameters of $Zn_{0.9}Cu_{0.1}S$ filled PVA/CMC/PEG blends

A. M. El-naggar¹ · Zein K. Heiba² · A. M. Kamal³ · Mohamed Bakr Mohamed^{2,4}

Received: 7 April 2023 / Accepted: 13 June 2023 / Published online: 30 June 2023

© The Author(s), under exclusive licence to Springer Science+Business Media, LLC, part of Springer Nature 2023

Abstract

Casting and solid-state reaction methods were used to prepare composites of PVA/CMC/PEG/x wt% $Zn_{0.9}Cu_{0.1}S$ ($x=0, 1, 3, 5, 10$). The nanofiller $Zn_{0.9}Cu_{0.1}S$ was investigated applying XRD Rietveld analysis. XRD, FTIR, SEM, and EDS techniques were used to trace the variation of the structure and morphology of the PVA/CMC/PEG blend upon loading with different $Zn_{0.9}Cu_{0.1}S$ contents. The effect of the filler content (x) on the linear and nonlinear features of the host blend was examined. The direct and indirect optical band gaps of PVA/CMC/PEG (5.87 and 5.31 eV) reduced upon loading with $Zn_{0.9}Cu_{0.1}S$, attaining minimum values (4.47 and 3.65 eV) for $x=10\%$. The fluorescence intensity and the emitted colors of the blends depended on the amount of the nanofiller. The dielectric constant (ϵ'), dielectric loss factor (ϵ''), the real (M') and imaginary (M'') parts of the electric modulus changed nonmonotonically with the nanofiller content (x). Among all blends, ϵ' disclosed higher values for the blend with $x=10$ wt% and lowest ones for $x=1$ wt%, while ϵ'' attained highest values for the blend with $x=3$ wt%, and lowest values for $x=5$ wt%.

Keywords PVA/CMC/PEG · Nano $Zn_{0.9}Cu_{0.1}S$ doped amount · Structure, dielectric · Linear and nonlinear optical

✉ Mohamed Bakr Mohamed
mbm1977@yahoo.com

A. M. El-naggar
elnaggar@ksu.edu.sa

Zein K. Heiba
zein_kh@yahoo.com

A. M. Kamal
amgadmazhar@yahoo.com

¹ Research Chair of Exploitation of Renewable Energy Applications in Saudi Arabia, Physics and Astronomy Department, College of Science, King Saud University, P.O. Box 2455, Riyadh 11451, Saudi Arabia

² Physics Department, Faculty of Science, Ain Shams University, Cairo, Egypt

³ Physics and Astronomy Department, College of Science, King Saud University, P.O. Box 2455, Riyadh 11451, Saudi Arabia

⁴ Physics Department, Faculty of Science, Taibah University, Al-Madina Al Munawarah, Saudi Arabia

1 Introduction

Polymers offer numerous benefits, including high strength, flexibility, low cost, and excellent mechanical qualities. Polymeric nanocomposites, which are made up of organic polymers and inorganic materials and have been employed in a variety of important applications such as medical and nuclear protection (Guo et al. 2023).

Poly(vinyl alcohol) is a biodegradable polymer that doesn't have a smell or taste. It can be dissolved in water. PVA is a crystalline polymer and has an attic structure. PVA is made up of H-atoms in between the hydroxyl groups that are linked together. Additives could change the crystallinity of PVA (Verma et al. 2022). Due to the intrinsic molecular features of PEG (polyethylene glycol), which is used as a coating material for biotechnical applications, a PVA/PEG (polyvinyl alcohol/polyethylene glycol) blend represents a promising material for many applications and expands the applications of PVA (Alibwaini et al. 2022). A semicrystalline polysaccharide called cellulose gum (sodium salt-carboxymethyl cellulose; CMC) is present in the fibrous tissue of plants. This polymer can gel, combine with other water-soluble polymers, and effectively reacts with ionic dopants thanks to the -OH (hydroxyl) and COO (carboxylic anion) groups (Sayed and Saber 2022).

Among the II-VI semiconductors, ZnS has the largest direct band gap at 3.68 eV (D'Amico 2017), making it one of the most important materials in the field. The wide direct bandgap of ZnS has made it a popular host matrix for numerous types of doping agents over the past two decades.

By incorporating the appropriate kind of dopant, the performance of a polymer or blended polymer can be modified. For example, after the addition of multi-walled carbon nanotubes/zinc oxide nanoparticles, polyethylene oxide/polyvinyl alcohol blend films formed a promising material for optoelectronic device applications (Alzahrani et al. 2022). It is possible to create novel NiO/CMC-PVP nanocomposites with greatly enhanced refractive index, reduced band gap, and improved conductivity. As a result, these materials are appropriate for engineering, electrochemical, and optoelectronic uses, as well as coatings and lenses (Sayed and Saber 2022). The addition of cellulose nanofibers promotes the uniform dispersion of SiO₂ NP and increases the CMC's toughness and rigidity (Saha et al. 2019). After doping with 0.0–0.8 wt% ZnO nanorods, some improvements were made to the thermal and dielectric properties of CMC(70%)–PVA(30%) (Abutalib 2019). Catalytic activity for the removal of organic and inorganic pollutants is enhanced in CuO/NiO/CMC nanocomposites compared to nano CuO–NiO (Maslamani et al. 2021). The AC conductivity of PVA was increased upon loading with 1.60 wt% of TiO₂/Cu nanoparticles, and the electrical modulus analysis indicated that the doped samples can be applied in energy storage capacitor and separator-rechargeable lithium-ion battery applications (Al-Hakimi et al. 2023). El sayed et al. (2015) found that Schottky emission is responsible for the low-temperature conduction in PVA/CMC films, while the Poole–Frenkel effect is important in CuO-doped films at higher temperatures. Interfacial bonding between V₂C MXene and wide-bandgap ZnS improves the dielectric response of ternary polymeric composite films (Deng et al. 2021). Nanocomposites with a silver doped ZnS core–shell were used to enhance photon harvesting in polymer cells (Ike et al. 2022). Arandhara et al. studied the consequences of Cu integration on the crystallinity, lattice strain, morphology, and electrical features of nanostructured ZnS-PVA thin films. They found that as Cu concentration rises, the optical band gap falls from 3.72 to 2.80 eV. The films have electrical resistivities on the order of 10⁸ cm at room temperature (Arandhara and Saikia 2021).

Due to their similar electronic shell structures, physical and chemical characteristics, Cu^{2+} replaces Zn^{2+} easily (Arandhara and Saikia 2021). Cu-doped ZnS thin films have lower electrical resistivity (Oztas et al. 2006). Cu changes ZnS thin film conductivity from n- to p-type (Daniela et al. 2014) and created new luminescence centers in ZnS nanocrystals.

The growing number of energy storage applications have highlighted the need for investigation into polymer nanocomposites based on nanofiller that exhibit high dielectric properties (Bera et al. 2023). PVA-CMC-PEG composite presented a spongy porous structure, excellent transparency, and good mechanical property due to hydrogen bond interaction between PVA, CMC and PEG (Li et al. 2019). In the present work, we aimed to upgrade the optical and electrical of PVA/CMC/PEG blend via loading with nano $\text{Zn}_{0.9}\text{Cu}_{0.1}\text{S}$ with different contents. The linear and nonlinear optical parameters as well as the emitted colors and dielectric properties of all blends were fully investigated.

2 Materials and methods

The $\text{Zn}_{0.9}\text{Cu}_{0.1}\text{S}$ sample was prepared by mixing and grinding zinc acetate (Sigma Aldrich), copper acetate (Sigma Aldrich), and thiourea for 6 h at a stoichiometric ratio (0.9:0.1:1). The powder was heated at 300 °C (3 h) in an electric oven. PVA/CMC/PEG blended polymer was formed by casting: 0.7, 0.15, and 0.15 g of polyvinyl alcohol (PVA), carboxymethyl cellulose (CMC) (in the form of the sodium salt of commercial grade), and polyethylene glycol (PEG) were dissolved in 70, 15, and 15 ml of distilled water at 70 °C, 50 °C, and room temperature (RT), respectively. After that, all three solutions were mixed at room temperature for 5 h. The last solution was put in a Petri dish and placed in an electric furnace for 5 days at 40 °C. PVA/CMC/PEG/*x* wt% $\text{Zn}_{0.9}\text{Cu}_{0.1}\text{S}$ (*x*=0, 1, 3, 5, 10) blended polymers were prepared by repeating the previous procedure with different wt% of the $\text{Zn}_{0.9}\text{Cu}_{0.1}\text{S}$ sample. Blended polymers of PVA/CMC/PEG/*x* wt% $\text{Zn}_{0.9}\text{Cu}_{0.1}\text{S}$ (*x*=0, 1, 3, 5, 10) were made by simply repeating the process with different wt% of $\text{Zn}_{0.9}\text{Cu}_{0.1}\text{S}$. The resulting blends are between 0.18 and 0.24 mm (digital micrometer with accuracy $\pm 1 \mu\text{m}$) in thickness.

Using a PANalytical diffractometer (X'pert MPD, Philips, copper source), the x-ray diffraction spectra were gathered. The structural and microstructural parameters of the powder filler were determined by applying the Rietveld method implemented in MAUD program (Rodríguez-Carvajal 1993; Lutterotti 2010). The morphology, compositions, and vibration bands of different samples were collected by Fourier transform infrared (FTIR) spectroscopy (Bruker Tensor 27 FTIR Spectrometer) and scanning electron microscopy (JEOL, Akishima, Tokyo, Japan, JED-2200 Series). The optical characteristics were discovered by a luminescence spectrophotometer (FP-8200 JASCO) and diffused reflectance spectrophotometer (JASCO-V-670) with attached integrating sphere assembly techniques.

Capacitance (*C*) and dissipation factor/ $\tan\delta$ under applied ac voltage (2 V) for the various blends (in the form of a circular disk with a diameter (*D*) of 13 mm and a thickness (*d*) of 0.18–0.24 mm) were measured using the LCR-8105G device to determine the change in the dielectric constant at room temperature with frequency ($f=100 \text{ Hz}-1 \text{ MHz}$). The subsequent formula (Sharma et al. 2016) was used to find the real (ϵ') and imaginary (ϵ'') components of the dielectric constant, the ac conductivity (σ_{ac}), and the complex electric modulus ($M^* = M' + iM''$) of all blends.

$$\epsilon' = dC/\epsilon_0 A \quad (1)$$

$$\sigma_{ac} = 2\pi f \epsilon_0 \epsilon' \tan \delta \quad (2)$$

$$\tan \delta = \epsilon''/\epsilon' \quad (3)$$

$$M' = \frac{\epsilon'}{\epsilon'^2 + \epsilon''^2} \quad (4)$$

$$M'' = \frac{\epsilon''}{\epsilon'^2 + \epsilon''^2} \quad (5)$$

where ϵ_0 and A are the permittivity of free space and area of the used blend, respectively.

3 Results and discussion

3.1 Structure investigations

Rietveld analysis of the x-ray diffraction pattern measured for the nanofiller $Zn_{0.9}Cu_{0.1}S$, Fig. 1a, proved a single ZnS phase of cubic zincblende structure, necessitating incorporation of Cu ions into the ZnS lattice. The refined cell parameter is 5.354(2) Å, the determined average crystallite size is 2.0 nm and the average lattice microstrain is 1.9×10^{-4} . The obtained diffraction patterns for the PVA/CMC/PEG polymer blends, pure and filled with different x wt% of $Zn_{0.9}Cu_{0.1}S$ ($x=0.0, 0.03, 0.05, \text{ and } 0.1$), are given in Fig. 1b. No characteristic peaks of ZnS could be seen, all patterns exhibited a high background due to diffuse scattering, superimposed with weak and broad peaks indicating a small degree of crystallinity of the polymer blends. The main broad peak around $2\theta=20^\circ$ resulted from the overlap of the characteristic peaks of PVA at $2\theta \sim 19.2^\circ$ and 20.2° (Golitsyn et al. 2019; Assender and Windle 1998) and those of PEG at $2\theta \sim 19.3^\circ$ and 23.5° (Hotaby et al. 2017; El-naggar et al. 2022a). The small, distinctive peak detected at around $2\theta=41.5^\circ$ is assigned to PVA (Assender and Windle 1998).

SEM images were recorded to follow the effect of loading the polymer blend PVA/CMC/PEG with $Zn_{0.9}Cu_{0.1}S$ on the surface morphology of the obtained films. Figure 1c, d depict the SEM image for pure and 10 wt% $Zn_{0.9}Cu_{0.1}S$ filled polymer blends. A smooth, homogenous surface could be seen for the pure polymer blend, there are some white patches appeared, manifesting the partial immiscibility of the PVA/CMC/PEG blend. Upon loading, the surface attained some roughness. Figure 2 shows EDS analysis for pure and 10 wt% $Zn_{0.9}Cu_{0.1}S$ filled polymer blends. The figure also represented the element percentages in each blend.

Figure 3 displays the FTIR data for pure and filled PVA/CMC/PEG blends with various amounts of $Zn_{0.9}Cu_{0.1}S$. The diagram shows that the intensity and location of vibration bands in the blends vary with the $Zn_{0.9}Cu_{0.1}S$ content of the blends. Cyriac et al. explained the variations in the wavenumbers/intensity of FTIR for PVA/CMC doped with NaI salt due to the cationic coordination of free Na^+ dissociated from NaI salt with the oxygen atom of the OH group via Lewis acid–base interaction. i.e. $Na^+ \cdots OH$ (Cyriac et al. 2022). These variations indicated that the host polymer and the filler are coupled and formed new bonds

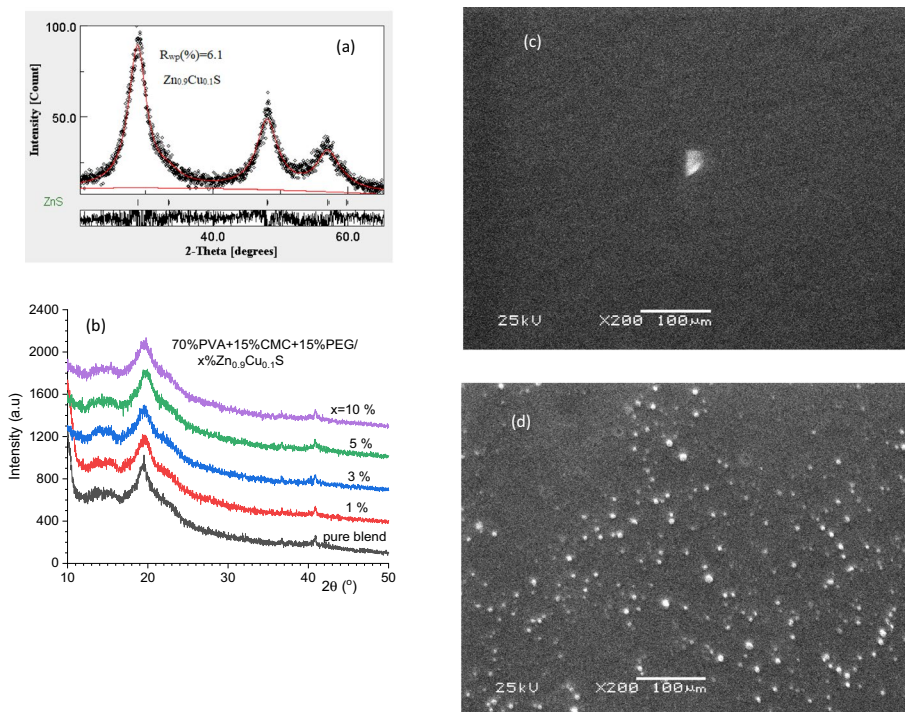


Fig. 1 **a** Rietveld analysis for $Zn_{0.9}Cu_{0.1}S$, **b** XRD spectra for PVA/CMC/PEG/ x wt % $Zn_{0.9}Cu_{0.1}S$ blends and **(c, d)** SEM images for undoped and doped PVA/CMC/PEG blend with 10 wt% $Zn_{0.9}Cu_{0.1}S$

between them. Additionally, the wide peak at $3767\text{--}3785\text{ cm}^{-1}$ is an OH stretching bond (Rajeswari et al. 2014). The vibration bands at 2209, 2026 and 1868 cm^{-1} were connected to the $C\equiv C$, $C\equiv N$ and $C=O$ bonds, respectively (Farah et al. 2012; Xia et al. 2010; Morsi et al. 2019).

3.2 UV-Spectroscopy study

The changes in absorption, transmittance, and reflectance data of pure and filled PVA/CMC/PEG blends with different amounts of $Zn_{0.9}Cu_{0.1}S$ are depicted in Fig. 4. The absorption band and shoulder at 199 and 324 nm in the pure and doped PVA/CMC/PEG blends can be attributed to the $n\rightarrow\pi^*$ electronic transition (oxazine rings in the blended system) and the main $\pi\rightarrow\pi^*$ type transitions, respectively (Alrebdy et al. 2022). The absorbance of the blend increased as the quantity of nanofiller rose, Fig. 4a. In addition, when compared to an undoped blend, the absorption band of the doped blend is red shifted, Fig. 4a. The same thing was found when the amounts of natural melanin doping were increased in PVA/PVP blend, the absorbance increased (El-naggar et al. 2023a). This change could be explained by the doped blends' developing internal molecular bonds between various cations and anions. As a result, defects are produced in the matrix of the doped PVA/CMC/PEG blend. Additionally, compared to undoped blends, doped blends with varying amounts of $Zn_{0.9}Cu_{0.1}S$ had lower optical transmittance. As the $Zn_{0.9}Cu_{0.1}S$ content increased, the transmittance decreased (Fig. 4b). This reduction is attributable to a rise in

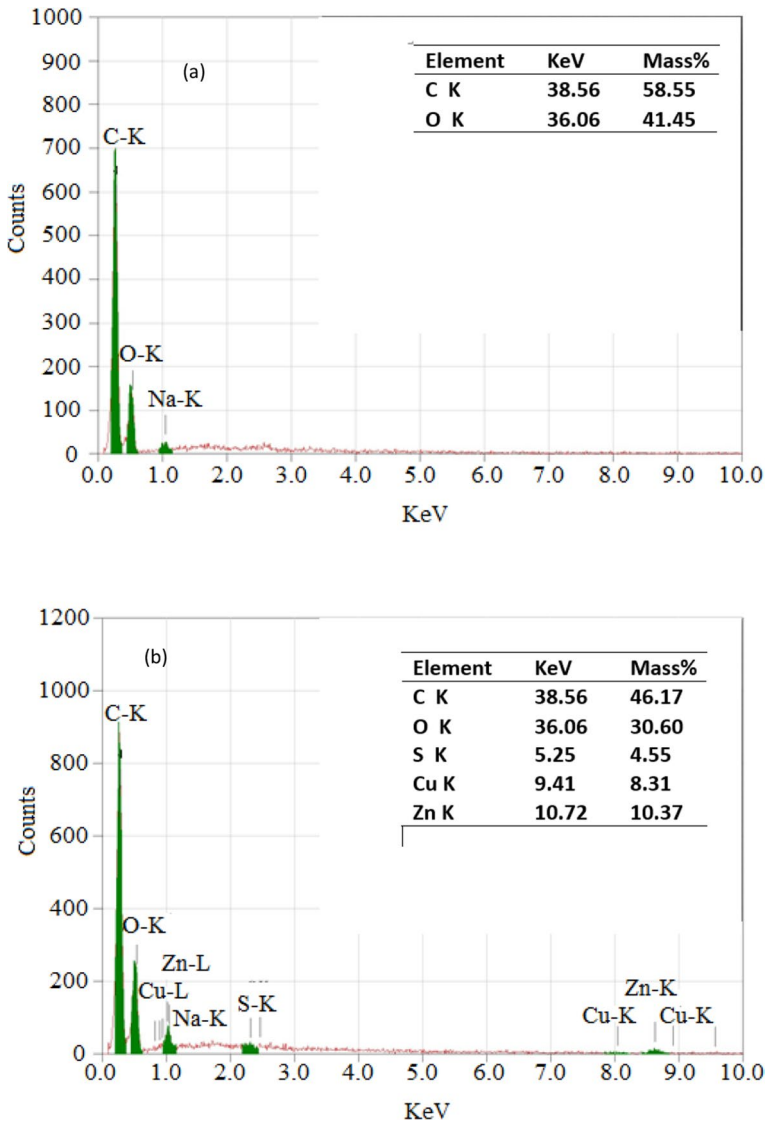


Fig. 2 EDS for **a** undoped PVA/CMC/PEG and **b** doped with $Zn_{0.9}Cu_{0.1}S$ blends

photon scattering from the dense nanoparticles in the blend. As the blend's $Zn_{0.9}Cu_{0.1}S$ content grew, the optical reflectance spectra improved, Fig. 4c.

The direct and indirect optical energy bandgap (E_g) values of all samples were obtained from the following expression (El-naggar et al. 2023b):

$$\alpha h\nu = B(h\nu - E_g)^q \quad (6)$$

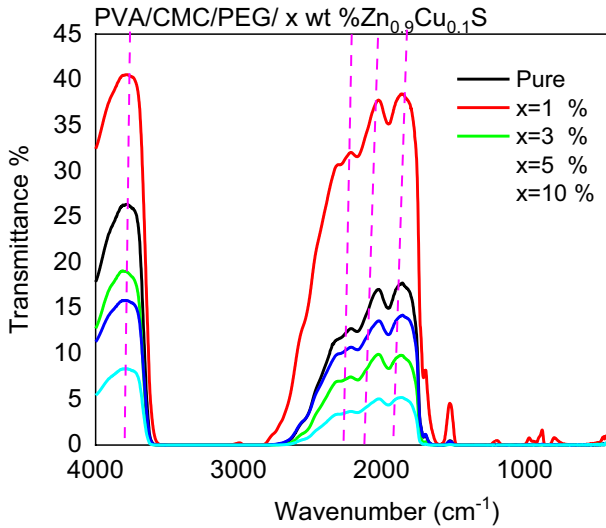


Fig. 3 FTIR for PVA/CMC/PEG/ x wt% $Zn_{0.9}Cu_{0.1}S$ blends

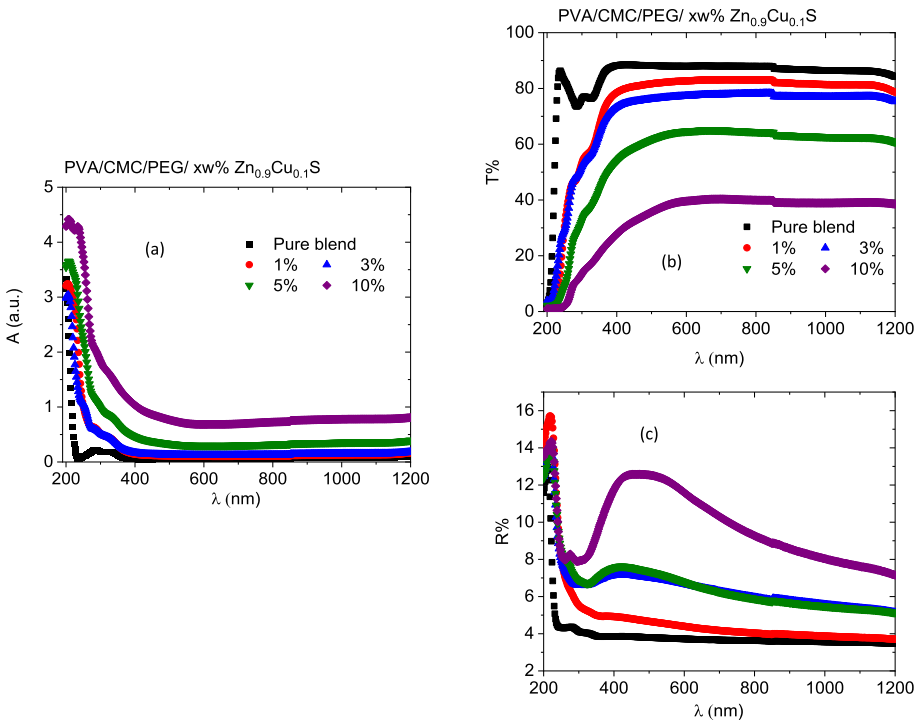


Fig. 4 **a** Absorbance, **b** transmittance and **c** reflectance data for PVA/PVP/CMC/ x wt% $Zn_{0.9}Cu_{0.1}S$ blends

where h, ν, B, α ($=2.303A/d$), and t are Planck’s constant, incident light frequency, a constant, absorption coefficient, and sample thickness, respectively. $q=0.5$ or 2 for direct and indirect optical band transitions, respectively.

By extrapolating the linear portion to the intercept with the x-axis in Fig. 5a, b, the optical band gap energy (direct (E_{dir}) or indirect (E_{ind})) is calculated. The addition of $Zn_{0.9}Cu_{0.1}S$ to PVA/CMC/PEG reduced E_{dir} and E_{ind} from 5.87 to 5.31 eV to minimum values of 4.47 and 3.65 eV as the blend was doped with 10% $Zn_{0.9}Cu_{0.1}S$, as revealed in Fig. 5c. Similar results were obtained as PVA doped with manganese chloride (Banerjee et al. 2019, 2018). This reduction is the result of changing the host blend’s degree of disorder, as well as the host blend’s number of defects increasing as the nanofiller concentration increased. As a result, the locally created state inside the optical band gap changed, having an impact on the optical band gaps (Sayed and Saber 2022).

The refractive index (n), extinction coefficient (k), real (ϵ_r) and imaginary (ϵ_i) dielectric constant parts of the various samples were determined by El-naggar et al. 2023b; El-naggar et al. 2022b):

$$n = \frac{1 + R}{1 - R} + \sqrt{\frac{4R}{(1 - R)^2} - k^2} \tag{7}$$

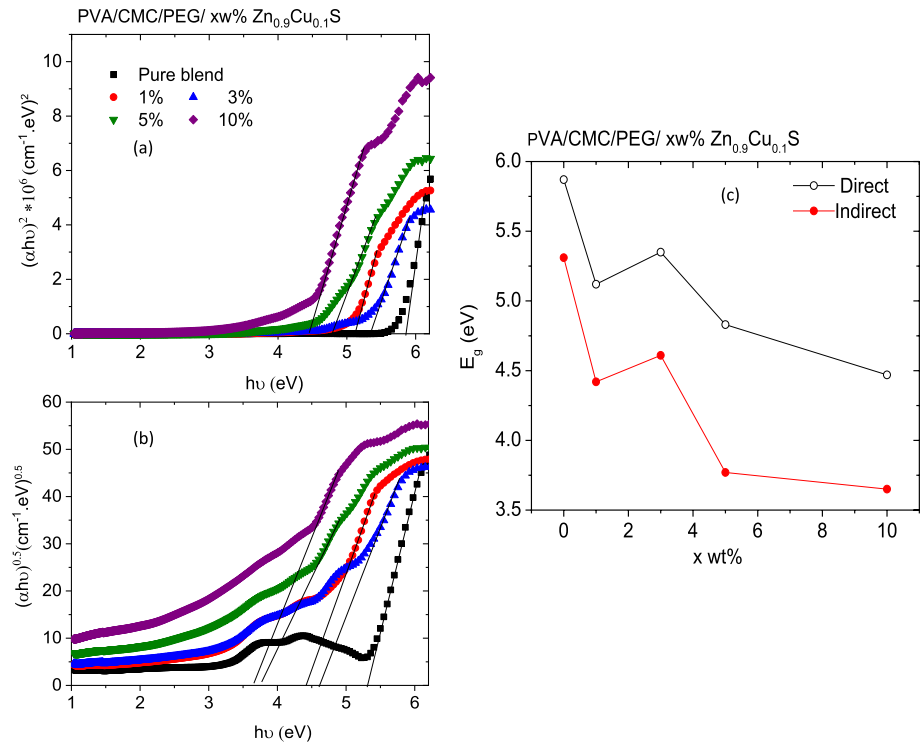


Fig. 5 a $(\alpha h\nu)^2$ and b $(\alpha h\nu)^{0.5}$ vs. the photon energy ($h\nu$) relations and c variation of optical band gaps for PVA/CMC/PEG/ x wt% $Zn_{0.9}Cu_{0.1}S$ blends

$$k = \frac{\lambda\alpha}{4\pi} \quad (8)$$

$$\varepsilon_r = n^2 - k^2 \quad (9)$$

$$\varepsilon_i = 2nk \quad (10)$$

As can be seen in Fig. 6a, the n value of the PVA/CMC/PEG blend exhibited a normal dispersion, where n decreased with increasing wavelength. The n value exhibited both normal and anomalous dispersion behaviors as $\text{Zn}_{0.9}\text{Cu}_{0.1}\text{S}$ was added in varying concentrations to the blend, decreasing first as the wavelength increased up to 300 nm, then increasing, and finally decreasing as the wavelength increased. Filling the blend with nanofiller increased its n value compared to the undoped blend. When a blend is doped with a nanofiller, the n value of the blend may change, which may affect the intramolecular bonding that has formed between nano $\text{Zn}_{0.9}\text{Cu}_{0.1}\text{S}$ and the blend matrix, and, as a result, the density of chain packing may change (El-Shamy 2021). Additionally, as the wavelength increased, the values of k for all blends diminished (Fig. 6b). As the PVA/CMC/PEG blend was filled with $\text{Zn}_{0.9}\text{Cu}_{0.1}\text{S}$ nanofiller, its k value increased. This change in the k value could be attributed to the absorption property of the blends after

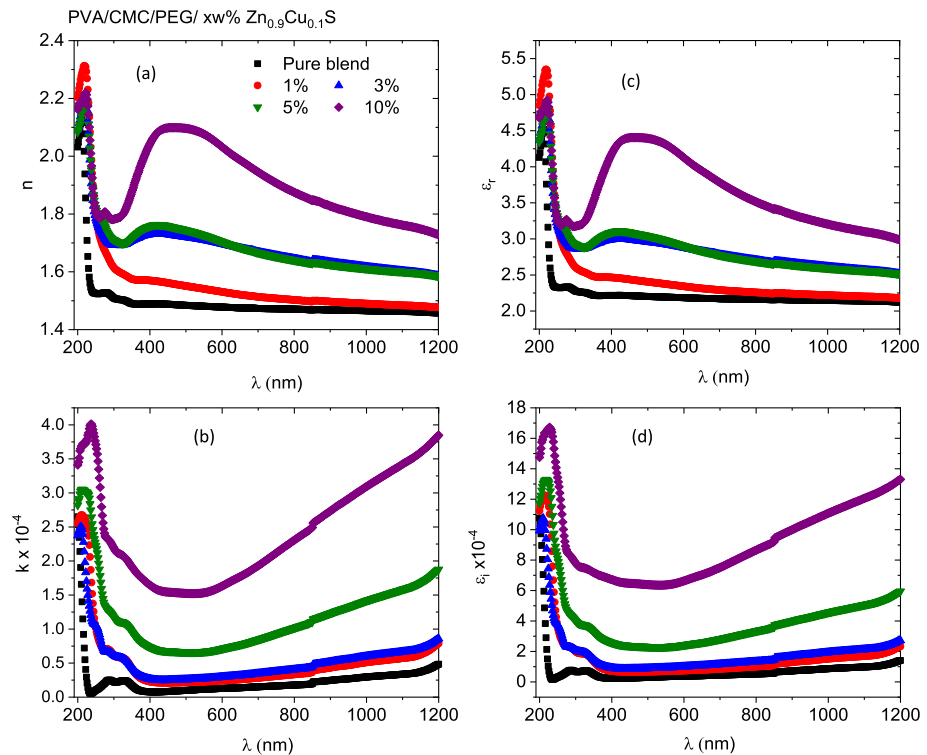


Fig. 6 The **a** refractive index, **b** extinction coefficient, **(c, d)** real and imaginary parts of the dielectric constant for PVA/CMC/PEG/ x wt% $\text{Zn}_{0.9}\text{Cu}_{0.1}\text{S}$ blends

filling with nanocrystal fillers, which alters the interaction between incident light and free carriers in filled blends (Tanaka 1980).

The wavelength dependence of the real part (ϵ_r) and imaginary part (ϵ_i) of the dielectric constant for pure and filled blends with varying amounts of $\text{Zn}_{0.9}\text{Cu}_{0.1}\text{S}$ is shown in Fig. 6c, d. The performances of ϵ_r and ϵ_i are similar to the corresponding n and k values of the different blends. Each blend has a larger value of ϵ_r than ϵ_i . A doped blend's ϵ_r and ϵ_i values are higher than those of a pure blend. Loading the blend with nanofillers may alter ϵ_r and ϵ_i values because of a change in the interaction between electrons in the blend and photons or a change in the dipole motion of the polymer as a result of filling with nano materials (Wise 1998; Suma et al. 2017). Miller's relations can be used to figure out three important nonlinear parameters, most of which are based on the blends' refractive indices. The parameters are the first-order nonlinear susceptibility ($\chi^{(1)}$), the nonlinear refractive index (n_2) and the third-order nonlinear susceptibility ($\chi^{(3)}$).

The linear optical susceptibility ($\chi^{(1)}$), nonlinear third order optical susceptibility ($\chi^{(3)}$), and nonlinear refractive index (n_2) of the various samples were determined from the next formula (El-naggar et al. 2023b, 2022b):

$$\chi^{(1)} = \frac{1}{4\pi} (n^2 - 1) \quad (11)$$

$$\chi^{(3)} = 1.7 * 10^{-10} (\chi^{(1)})^4 = 1.7 * 10^{-10} \left(\frac{n^2 - 1}{4\pi} \right)^4 \quad (12)$$

$$n_2 = \frac{12\pi}{n} \chi^{(3)} \quad (13)$$

where C is velocity of the light.

Figure 7 shows how the nonlinear parameters of the investigated blends vary with the wavelength of the incident photon. Based on these graphs, increasing the amount of $\text{Zn}_{0.9}\text{Cu}_{0.1}\text{S}$ made the NLO parameters of the PVA/CMC/PEG blend better. This could be a result of the blends' refractive indices improving, which also contributed to the blends' three-dimensional network expanding. This might suggest that the blends under investigation have extra carriers. Therefore, the nonlinear response to the electric field of incident light is enhanced. Similar results were detected as the amount of silver nitrate doping was increased in PVP/PVA polymer blends (Ali et al. 2021). Also, silver nanoparticles increased the nonlinear optical properties of PANI/MC blend polymers, and this was attributed to an improvement in the interaction between the nanofiller and the blend (Khan et al. 2019).

3.3 Fluorescence (FL) characteristics

Figure 8a displays the fluorescence (FL) data for unloaded PVA/CMC/PEG blend and those loaded with varying contents of $\text{Zn}_{0.9}\text{Cu}_{0.1}\text{S}$ under excitation wavelength of 317 nm. The pure PVA/CMC/PEG blend manifested a broad FL emission spectrum attaining maximum intensity at 2.96 eV. Also, the spectrum comprises a shoulder around 2.7 eV and a small peak at 3.52 eV. The spectrum is a collective result of the electronic transitions $\pi^* \rightarrow \pi$ and/or $\pi^* \rightarrow n$ of the functional groups of constituent polymers. The FL intensity is enhanced upon loading the PVA/CMC/PEG blend with x wt% $\text{Zn}_{0.9}\text{Cu}_{0.1}\text{S}$ reaching

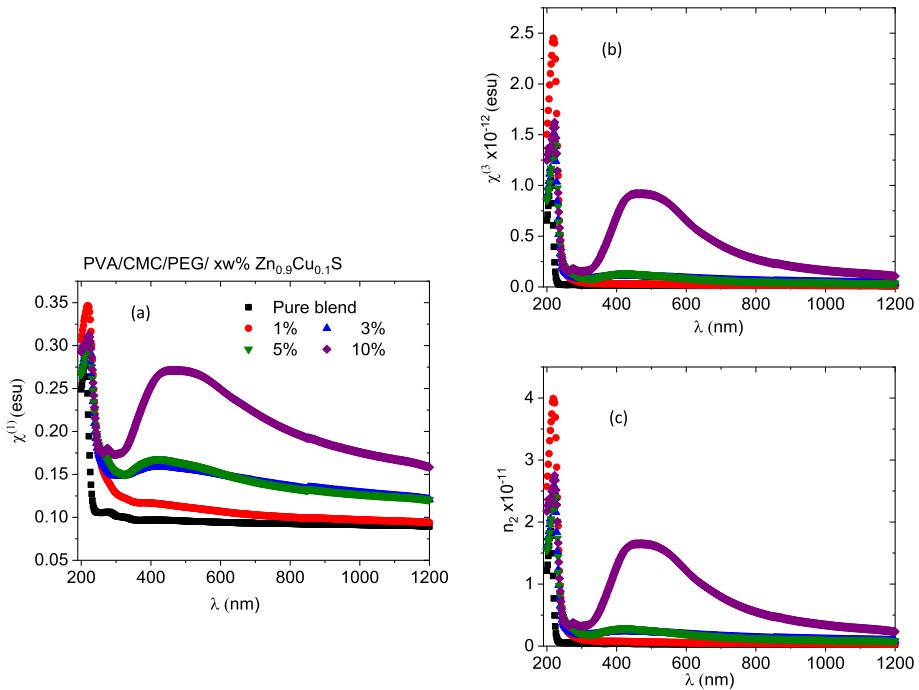


Fig. 7 The **a** linear optical susceptibility, **b** nonlinear third order and **c** nonlinear refractive index for PVA/CMC/PEG/ x wt% $Zn_{0.9}Cu_{0.1}S$ blends

maximum for $x=3\%$, then decreased for higher values of (x), Fig. 8a. Also, the position of spectrum maximum intensity is blue shifted. Similar FL enhancement was obtained upon loading PVA with ZnS (Khan et al. 2019). These results demonstrated the interaction between $Zn_{0.9}Cu_{0.1}S$ and the polymer blend, which comprehensively rearrange the delocalized n -electrons of the functional groups. The reduction in FL for higher nano filler content (x) is attributed to the concentration quenching (El-naggar et al. 2022c). The emitted colors from various blends can be found by means of Gaussian fitting (Fig. 8b, c). According to the fitting, the pure blend produced (two UV, two violets, blue, and green) colors, whereas the doped blends produced (UV, two violets, blue, and two green) colors. The excitonic transitions were related to UV and violet emissions. The formation of defects inside the various blends, dopant or impurity atoms, and defect-related luminescence, respectively, were the causes of the blue and green colors (El-naggar et al. 2022c).

3.4 Dielectric properties

Figure 9a, b displays the frequency dependence of the dielectric constant (ϵ') and dielectric loss factor (ϵ'') for PVA/CMC/PEG / x wt% $Zn_{0.9}Cu_{0.1}S$ blends. From the graph, one can notice that, for all blends, the ϵ' value was reduced as the frequency increased. The ϵ' high value in the low frequency range is due to the large number of charges gathering on the surface area of the blend (interfacial polarization). Besides, in the high frequency range, electrons and atoms show a displacement polarization, whereas interfacial and orientation polarizations are limited, producing a small charge on the blend's surface (Watanabe et al.

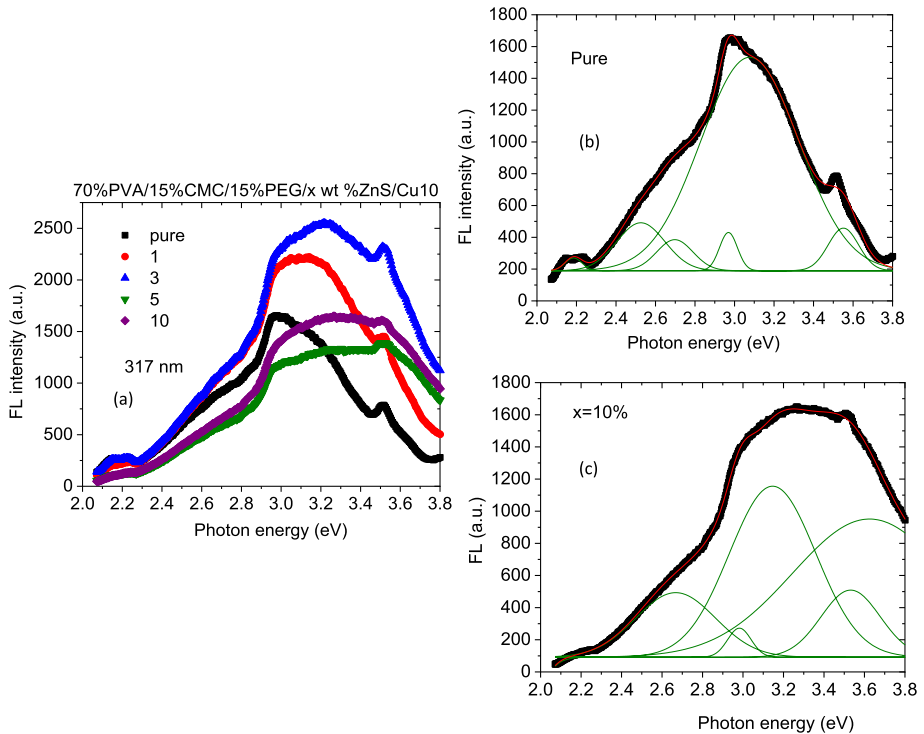


Fig. 8 a The FL spectra for PVA/CMC/PEG / x wt% Zn_{0.9}Cu_{0.1}S blends and (b, c) Gaussian fitting as an example

2020). As the content of Zn_{0.9}Cu_{0.1}S (x) increased, ϵ' displayed nonmonotonically changes. Compared to pure blend ($x=0$ wt%), ϵ' decreased for the blend $x=1$ wt%, increased for $x=3$ and 10 wt%, and decreased for $x=5$ wt%. On the other hand, ϵ'' first increased reaching a peak in the middle frequency range (α -relaxation peak) (Choudhary 2017), then reduced as the frequency increased. The peak location was shifted to the higher-frequency side with the filler content (x). This shift indicates a reduction in relaxation time (Boucher et al. 2012). Furthermore, for the blend with $x=3$ wt%, ϵ'' attained higher values compared with the pure blend for whole frequency range, while other blends attained lower ϵ'' values before α -relaxation peak and higher values after the peak.

The changes in AC electrical conductivity (σ_{AC}) with frequency for all the samples are illustrated in Fig. 9c. At lower frequencies, conductivity (σ_{AC}) tends to attain constant values (i.e., a frequency increase is not noticeable at the low frequency range) and is approaching DC values. It increased exponentially with increasing frequency after a certain value of frequency. Hopping transport between localized states is responsible for the frequency dependence of conductivity in polymer composites (Abdullah et al. 2016). In addition, as the amount of Zn_{0.9}Cu_{0.1}S increased, so did the σ_{AC} , except for the blend contained 5% wt Zn_{0.9}Cu_{0.1}S, it decreased.

This finding demonstrates that as the percentage of Zn_{0.9}Cu_{0.1}S in the blend rises, a greater number of polarons (electrons) are being added to the conducting pool. The variations of the real (M') and imaginary (M'') parts of the electric modulus with frequency are depicted

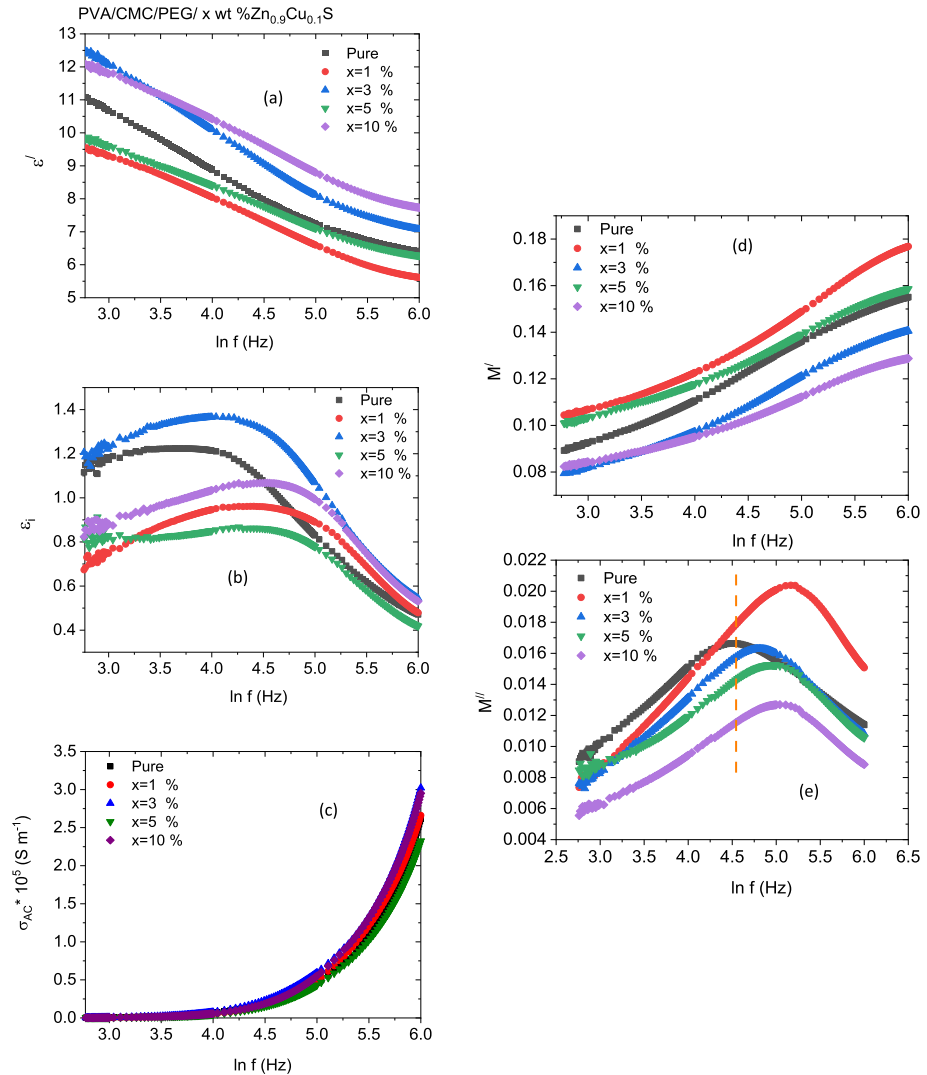


Fig. 9 a Real, b imaginary parts of the dielectric constant, c AC conductivity, d real and e imaginary parts of electric modulus for PVA/CMC/PEG / x wt% Zn_{0.9}Cu_{0.1}S blends

in Fig. 9d and e for all samples. For all blends, at low frequencies M' has a low value that increases with the frequency. In the presence of the applied field, this feature may be brought on by the weak restoring forces for the charge carrier (Prabu and Selvasekarapandian 2012). The evolution in M' may be explained by the conduction phenomenon associated with the short-range mobility of charge carriers (Alghunaim 2019). M' changed nonmonotonically with Zn_{0.9}Cu_{0.1}S content; compared with pure blend, it is increased for $x=1$ and 5 wt% and decreased for $x=3$ and 10 wt%. Furthermore, the value of the M'' starts low and gradually rises until it reaches its maximum value; after that, it diminishes as the frequency increases. The samples' ionic conductivity is established by the existence of a peak in the electrical

modulus. As the blend contained 5 or 10 wt% $\text{Zn}_{0.9}\text{Cu}_{0.1}\text{S}$, the intensity of this peak diminished, whereas it increased with other filling contents. This peak was also shifted to a higher frequency as the amount of $\text{Zn}_{0.9}\text{Cu}_{0.1}\text{S}$ changed. This exemplifies the contribution of nano $\text{Zn}_{0.9}\text{Cu}_{0.1}\text{S}$ to the relaxation process (Alghunaim 2019).

4 Conclusion

Composites of PVA/CMC/PEG blends loaded with nanofiller x wt% $\text{Zn}_{0.9}\text{Cu}_{0.1}\text{S}$ ($x = 1, 3, 5, 10$) have been prepared. XRD Rietveld analysis of powder $\text{Zn}_{0.9}\text{Cu}_{0.1}\text{S}$ revealed a nano cubic zincblende structure of average crystallite size of 2.0 nm. SEM micrographs of the obtained polymer composites disclosed a uniformly smooth surface with somewhat roughness after nanofiller loading. The absorbance of the blend is greatly enhanced as the content of nanofiller increased and the absorption band red shifted. The direct and indirect optical band gaps of PVA/CMC/PEG (5.87 and 5.31 eV) reduced upon loading with $\text{Zn}_{0.9}\text{Cu}_{0.1}\text{S}$, attaining minimum values (4.47 and 3.65 eV) for $x = 10$ wt%. Pure PVA/CMC/PEG blend exhibited normal dispersion, while doped blends revealed both normal and anomalous dispersion behaviors. Doped blends have higher n and optical dielectric values than the undoped blend. Upon increasing the $\text{Zn}_{0.9}\text{Cu}_{0.1}\text{S}$ content, the NLO parameters improved. The FL intensity is enhanced upon nanofiller loading, reaching maximum for $x = 3$ wt% then decreased for higher values of (x) due to the concentration quenching. A pure blend produced (two UV, two violets, blue, and green) colors, whereas the doped blends produced (UV, two violets, blue, and two greens) colors. The dielectric constant (ϵ'), dielectric loss factor (ϵ''), the real (M') and imaginary (M'') parts of the electric modulus changed nonmonotonically with the nanofiller content (x). Among all blends, ϵ' disclosed higher values for the blend with $x = 10$ wt% and lowest ones for $x = 1$ wt%, while ϵ'' attained highest values for the blend with $x = 3$ wt%, and lowest values for $x = 5$ wt%. As the $\text{Zn}_{0.9}\text{Cu}_{0.1}\text{S}$ content increased, the σ_{AC} increased, except the blend with $x = 5$ wt%. This exemplifies the contribution of nano $\text{Zn}_{0.9}\text{Cu}_{0.1}\text{S}$ to the relaxation process.

Acknowledgements The authors extend their appreciation to the Deputyship for Research & Innovation, Ministry of Education in Saudi Arabia for funding this research. (IFKSURC-1-1012).

Author contributions All authors have contributed, discussed the results and approved the final manuscript.

Funding This work is supported by Research & Innovation, Ministry of Education in Saudi Arabia.

Data availability The authors confirm that the data supporting the findings of this study are available within the article.

Declarations

Conflict of interest The authors declare that they have no conflict of interest.

Ethical approval We agreed all terms and conditions for Ethics approval.

References

Abdullah, O.G., Salman, Y.A.K., Saleem, S.A.: Electrical conductivity and dielectric characteristics of in situ prepared PVA/HgS nanocomposite films. *J. Mater. Sci.: Mater. Electron.* **27**, 3591–3598 (2016)

- Abutalib, M.M.: Effect of zinc oxide nanorods on the structural, thermal, dielectric and electrical properties of polyvinyl alcohol/carboxymethyl cellulose composites. *Phys. B* **557**, 108–116 (2019)
- Alghunaim, N.S.: Effect of CuO nanofiller on the spectroscopic properties, dielectric permittivity and dielectric modulus of CMC/PVP nanocomposites. *J. Mater. Res. Technol.* **8**(4), 3596–3602 (2019)
- Al-Hakimi, A.N., Asnag, G.M., Alminderej, F., Alhagri, I.A., Al-Hazmy, S.M., Qahtan, T.F.: Enhancing the structural, optical, thermal, and electrical properties of PVA filled with mixed nanoparticles (TiO₂/Cu). *Crystals* **13**, 135(1–17) (2023)
- Alibwaini, Y.A., Hemeda, O.M., Sharshar, T., Ashour, A.H., Abdul-Wali Ajlouni, E.A., Arrasheed, A.M.A., Henaish, R.E.-S.: Study of the PEG content effect on some properties of the PVA/PEG-EY films using the Raman, positron annihilation and impedance spectroscopies. *Optik* **254**, 168591(1–13) (2022)
- Alrebbdi, T.A., Ahmed, H.A., Alrefaee, S.H., Ad Pashameah, R., Toghan, A., Mostafa, A.M., Alkallas, F.H., Rezk, R.A.: Enhanced adsorption removal of phosphate from water by Ag-doped PVA-NiO nanocomposite prepared by pulsed laser ablation method. *J. Mater. Res. Technol.* **20**, 4356–4364 (2022)
- Alzahrani, H.S., Al-Sulami, A.I., Alsulami, Qana A., Rajeh, A.: A systematic study of structural, conductivity, linear, and nonlinear optical properties of PEO/PVA-MWCNTs/ZnO nanocomposites films for optoelectronic applications. *Opt. Mater.* **133**, 112900 (1–9) (2022)
- Arandhara, G., Saikia, P.K.: Effect of Cu incorporation on the crystallinity, lattice strain, morphology and electrical properties of nanostructured ZnS-PVA thin films. *Phys. B* **610**, 412924 (1–11) (2021)
- Assender, H.E., Windle, A.H.: Crystallinity in poly(vinyl alcohol). 1. An X-ray diffraction study of atactic PVOH. *Polymer* **39**, 4295–4302 (1998)
- Banerjee, M., Jain, A., Mukherjee, G.S.: Spectroscopic evaluation of optical parameters of a transition metal salt filled polymer material. *Defence Sci. J.* **68**(2), 225–231 (2018)
- Banerjee, M., Jain, A., Mukherjee, G.S.: Microstructural and optical properties of polyvinyl alcohol/manganese chloride composite film. *Polym. Compos.* **40**(S1), E765–E775 (2019)
- Bera, S., Singh, M., Thantirige, R., Tiwary, S.K., Shook, B.T., Nieves, E., Raghavan, D., Karim, A., Pradhan, N.R.: 2D-nanofiller-based polymer nanocomposites for capacitive energy storage applications. *Small Sci.* **2300016**, 1–28 (2023)
- Boucher, V.M., Cangialosi, D., Alegria, A.: Time dependence of the segmental relaxation time of poly(vinyl acetate)-silica nanocomposites. *J. Colmenero Phys. Rev. E.* **86**, 41501(1–10) (2012)
- Choudhary, S.: Dielectric dispersion and relaxations in (PVA-PEO)-ZnO polymer nanocomposites. *Phys. B* **522**, 48–56 (2017)
- Cyriac, V., Ismayil, I.M., Noor, K.M., Chavan, C., Bhajantri, R.F., Masti, S.P.: Ionic conductivity enhancement of PVA: carboxymethyl cellulose poly-blend electrolyte films through the doping of NaI salt. *Cellulose* **29**, 3271–3291 (2022)
- D'Amico, P., Calzolari, A., Ruini, A., Catellani, A.: New energy with ZnS: novel applications for a standard transparent compound. *Sci. Rep.* **7**, 16805, 1–9 (2017). <https://doi.org/10.1038/s41598-017-17156-w>
- Daniela, E., Ramos, O., Gonzalez, L.A., Bon, R.R.: p-Type transparent Cu doped ZnS thin films by the chemical bath deposition method. *Mater. Lett.* **124**, 267–270 (2014)
- Deng, Q., Xiong, W., Mao, B., Bo, M., Feng, Y.: Enhanced dielectric response of ternary polymeric composite films via interfacial bonding between V2C MXene and wide-bandgap ZnS. *Ceram. Int.* **47**, 32938–32946 (2021)
- El Sayed, A.M., Saber, S.: Structural, optical analysis, and Poole-Frenkel emission in NiO/CMC-PVP: bio-nanocomposites for optoelectronic applications. *J. Phys. Chem. Solids* **163**, 110590 (1–12) (2022)
- El Hotaby, W., Sherif, H.H.A., Hemdan, B.A., Khalil, W.A., Khalil, S.K.H.: Assessment of in situ-prepared polyvinylpyrrolidone-silver nanocomposite for antimicrobial applications. *Acta Phys. Pol.* **131**(6), 1554–1560 (2017)
- El Sayed, A.M., El-Gamal, S., Morsi, W.M., Mohammed, G.: Effect of PVA and copper oxide nanoparticles on the structural, optical, and electrical properties of carboxymethyl cellulose films. *J. Mater. Sci.* **50**, 4717–4728 (2015)
- Elhosiny Ali, H., Abd-Rabboh, H.S.M., Awwad, N.S., Algarni, H., Sayed, M.A., Abd El-Rehim, A.F., Abdel-Aziz, M.M., Khairy, Yasmin: Photoluminescence, optical limiting, and linear/nonlinear optical parameters of PVP/PVAL blend embedded with silver nitrate. *Optik* **247**, 167863(1–14) (2021).
- El-naggar, A.M., Heiba, Z.K., Kamal, A.M., Altowairqi, Y., Mohamed, M.B., Abd-Elkader, O.H., Alhazime, A.A.: Influence of nanocomposite (1-x) CdS/xCuS on optical characteristics of PVA/CMC/PEG blended polymer; effect of ratio (x). *Opt. Mater.* **133**, 112923 (1–12) (2022a)
- El-naggar, A.M., Heiba, Z.K., Mohamed, M.B., Kamal, A.M., Lakshminarayana, G.: Thermal, linear and nonlinear optical properties of PVA/PVP/PEG blends loaded with novovanadium-doped nano tin disulfide. *J. Mater. Sci.: Mater. Electron.* **33**(34), 25743–25752 (2022). <https://doi.org/10.1007/s10854-022-09267-6>

- El-naggar, A.M., Heiba, Z.K., Kamal, A.M., Lakshminarayana, G., Abd-Elkader, O.H., Mohamed, M.B.: Preparation of PVA/CMC/PVP blended polymer loaded with ZnS1-xCux; investigation of structural and linear/nonlinear optical properties. *Opt. Mater.* **133**, 113066 (1–11) (2022c)
- El-naggar, A.M., Heiba, Z.K., Kamal, A.M., Alzahrani, K.E., Abd-Elkader, O.H., Mohamed, M.B.: Impact of natural melanin doping on the structural, optical and dielectric characteristics of the PVP/CMC blend. *J. Taibah Univ. Sci.* **17**(1), 2190731 (1–11) (2023a)
- El-naggar, A.M., Heiba, Z.K., Kamal, A.M., Abd-Elkader, O.H., Lakshminarayana, G., Mohamed, M.B.: Linear and nonlinear optical characteristics of PVA/CMC/PEG blended polymer loaded with ZnS formed at different temperatures. *J. Mater. Sci.: Mater. Electron.* **34**, 114 (1–13) (2023). <https://doi.org/10.1007/s10854-022-09460-7>
- El-Shamy, A.G.: The optical anatomy of new polyvinyl alcohol/zinc peroxide (PVA/ZnO₂) nanocomposite films for promising optical limiting applications. *Prog. Org. Coat.* **150**, 105981(1–13) (2021)
- Farah, A.M., Thema, F.T., Dikio, E.D.: Synthesis of prussian blue and its electrochemical detection of hydrogen peroxide based on cetyltrimethylammonium bromide (CTAB) modified glassy carbon electrode. *Int. J. Electrochem. Sci.* **8**, 12132–12146 (2013)
- Golitsyn, Y., Pulst, M., Samiullah, M.H., Busse, K., Kressler, J., Reichert, D.: Crystallization in PEG networks: the importance of network topology and chain tilt in crystals. *Polymer* **165**, 72–82 (2019)
- Guo, Y., Ruan, K., Wang, G., Gu, J.: Advances and mechanisms in polymer composites toward thermal conduction and electromagnetic wave absorption. *Sci. Bulletin.* **68**(11), 1195–1212 (2023). <https://doi.org/10.1016/j.scib.2023.04.036>
- Ike, J.N., Adediji, M.A., Mola, G.T.: Silver doped ZnS core-shell nanocomposites to promote photon harvesting in polymer cells. *Phys. B* **646**, 414347(1–8) (2022)
- Khan, M.M.R., Pal, S., Hoque, M.M., Alam, M.R., Younus, M., Kobayashi, H.: Simple fabrication of PVA–ZnS composite films with superior photocatalytic performance: enhanced luminescence property, morphology, and thermal stability. *ACS Omega* **4**, 6144–6153 (2019)
- Li, Y., Zhu, C., Fan, D., Rongzhan, F., Ma, P., Duan, Z., Li, X., Lei, H., Chi, L.: Construction of porous sponge-like PVA-CMC-PEG hydrogels with pH-sensitivity via phase separation for wound dressing. *Int. J. Polym. Mater. Polym. Biomater.* **69**(8), 505–515 (2019). <https://doi.org/10.1080/00914037.2019.1581200>
- Lutterotti, L.: Total pattern fitting for the combined size–strain–stress–texture determination in thin film diffraction. *Nucl. Inst. Methods Phys. Res. B* **268**, 334–340 (2010)
- Maslamani, N., Khan, S.B., Danish, E.Y., Bakhsh, E.M., Zakeeruddin, S.M., Asiri, A.M.: Carboxymethyl cellulose nanocomposite beads as super-efficient catalyst for the reduction of organic and inorganic pollutants. *Int. J. Biol. Macromol.* **167**, 101–116 (2021)
- Morsi, M.A., Oraby, A.H., Elshahawy, A.G., Abd El-Hady, R.M.: Preparation, structural analysis, morphological investigation and electrical properties of gold nanoparticles filled polyvinyl alcohol/carboxymethyl cellulose blend. *J. Mater. Res. Technol.* **8**(6), 5996–6010 (2019)
- Oztas, M., Bedir, M., Yazici, A.N., Kafadar, E.V., Toktamis, H.: Characterization of copper-doped sprayed ZnS thin films. *Physica B* **381**, 40–46 (2006)
- Prabu, M., Selvasekarapandian, S.: Dielectric and modulus studies of LiNiPO₄. *Mater. Chem. Phys.* **134**(1), 366–370 (2012)
- Rajeswari, N., Selvasekarapandian, S., Sanjeeviraja, C., Kawamura, J., Bahadur, S.A.: A study on polymer blend electrolyte based on PVA/PVP with proton salt. *Polym. Bull.* **71**, 1061–1080 (2014)
- Rodríguez-Carvajal, J.: Recent advances in magnetic structure determination by neutron powder diffraction. *Phys. B* **192**, 55–69 (1993)
- Saha, N., Shah, R., Gupta, P., Mandal, B.B., Alexandrova, R., Sikiric, M.D., Saha, Petr: PVP - CMC hydrogel: an excellent bioinspired and biocompatible scaffold for osseointegration. *Mater. Sci. Eng.: C* **95**, 440–449 (2019). <https://doi.org/10.1016/j.msec.2018.04.050>
- Sharma, S., Basu, T., Shahee, A., Singh, K., Lalla, N.P., Sampathkumaran, E.V.: Complex dielectric and impedance behavior of magnetoelectric Fe₂TiO₅. *J. Alloys Compd* **663**, 289–294 (2016)
- Suma, G.R., Subramani, N.K., Shilpa, K.N., Sachhidananda, S., Satyanarayana, S., Siddaramaiah, S.V.: Effect of Ce_{0.5}Zr_{0.5}O₂ nano fillers on structural and optical behaviors of poly(vinyl alcohol). *J. Mater. Sci.: Mater. Electron.* **28**(14), 10707–10714 (2017). <https://doi.org/10.1007/s10854-017-6846-1>
- Tanaka, K.: Optical properties and photoinduced changes in amorphous as-S films. *Thin Solid Films* **66**, 271–279 (1980)
- Verma, S., Pandey, K.K., Mohan, C., Tripathi, M., Pawar, N.R.: Study of solute–solvent interaction in the solutions of PVA with PEG at 338 K by ultrasonic technique. *Mater. Today: Proc.* **67**(5), 811–815 (2022)

- Watanabe, S., Pilkington, G.A., Oleshkevych, A., Pedraz, P., Radiom, M., Welbourn, R., Rutland, M.W.: Interfacial structuring of non-halogenated imidazolium ionic liquids at charged surfaces: effect of alkyl chain length. *Phys. Chem. Chem. Phys.* **22**(16), 8450–8460 (2020)
- Wise, D.L.: *Electrical and Optical Polymer Systems: Fundamentals: Methods, and Applications*. CRC Press, Boca Raton (1998)
- Xia, Q., Zhao, X.J., Chen, S.J., Ma, W.Z., Zhang, J., Wang, X.L.: Effect of solution-blended poly(styrene-co-acrylonitrile) copolymer on crystallization of poly(vinylidene fluoride). *Express Polym. Lett.* **4**(5), 284–291 (2010)

Publisher's Note Springer Nature remains neutral with regard to jurisdictional claims in published maps and institutional affiliations.

Springer Nature or its licensor (e.g. a society or other partner) holds exclusive rights to this article under a publishing agreement with the author(s) or other rightsholder(s); author self-archiving of the accepted manuscript version of this article is solely governed by the terms of such publishing agreement and applicable law.